ChemComm

An alternate synthetic pathway to nanoscopic Li_2FeS_2 for energy storage

Journal:	*ChemComm*
Manuscript ID	CC-COM-09-2024-004748.R1
Article Type:	Communication

SCHOLARONE™
Manuscripts

Please do not adjust margins

ChemComm

COMMUNICATION

An alternate synthetic pathway to nanoscopic Li_2FeS_2 for energy storage

Received 00th January 20xx,
Accepted 00th January 20xx

DOI: 10.1039/x0xx00000x

Ryan H. DeBlock,[a] Hunter O. Ford,[b] Meghanne E. Tighe,[c] Debra R. Rolison,[a] and Jeffrey W. Long*[a]

Lithium-rich iron sulphide, Li_2FeS_2, exhibits reversible charge-storage via both cationic and anionic sites, storing nearly 400 mAh g^{-1}, but its synthesis is limited to solid-state methods that result in large primary particles. We describe an alternate solution-based, redox-mediated method to lithiate pyrite FeS_2, ultimately forming Li_2FeS_2.

Intercalation cathodes utilized in lithium-ion batteries (LIBs) rely on topotactic insertion and deinsertion of Li^+ from the material concomitant with transition-metal reduction and oxidation, respectively.[1] This insertion chemistry is typically limited to a one-electron transfer, determined by the moles of Li^+ in the cathode material and the available oxidation states in its transition metal. Recently, a class of lithium-rich oxides (e.g., Li_2RuO_3 and Li_2MnO_3) has demonstrated both cationic and anionic redox upon lithium insertion that can effectively double the capacity for a given material.[2,3] Research on the anion-redox mechanism predominantly focuses on characterizing and optimizing oxide-based materials. Due to the high voltages at which oxide-based anion redox is active, charge-storage processes may compete with electrolyte degradation and irreversible evolution of CO_2, CO, and O_2.[4,5]

In contrast with Li-rich oxide materials, analogous metal sulphides oxidize at lower and more practical voltages due to the higher energy of their frontier orbitals.[6-8] These alkali-rich chalcogenides present an attractive opportunity to avoid electrolyte breakdown, eliminate unsafe O_2 evolution, and provide a more stable electrochemical window in which to characterize the anionic-redox mechanism. One promising cathode composition, lithium-rich iron sulphide, Li_2FeS_2, stores 1.5 to 2 electrons per formula unit through coupled cation–anion redox that increases the achievable cathode capacity to nearly 400 mAh g^{-1}.[9,10] In contrast, lithium nickel manganese cobalt oxide (NMC) and nickel cobalt aluminium oxide (NCA) cathodes found in state-of-the-art LIBs typically store ~200 mAh g^{-1}.[11]

The synthesis of lithium-rich iron sulphide and related materials has historically been limited to high temperature (>880°C), solid-state methods that typically involve grinding and heating precursor materials (e.g., FeS_2, Fe, and Li_2S) to their molten state.[9-10,12,13] After cooling back to ambient temperature, the resulting materials are chunky particulates (tens of microns) that are difficult to further process into powder-composite electrodes for battery use. This melt-based approach also limits synthetic control for desired compositional variations (e.g., metal-site substitution for Fe in Li_2FeS_2) based on the melting points of other available precursors.

We describe an alternate synthetic route to Li_2FeS_2 based on selective chemical lithiation of pyrite FeS_2. Although FeS_2 can form Li_2FeS_2 electrochemically, it only does so at suitably low discharge rates and/or high temperatures corresponding to Equations (1) and (2).[14]

$$2Li + FeS_2 \longrightarrow Li_2FeS_2 \quad (1)$$

$$2Li + Li_2FeS_2 \longrightarrow 2Li_2S + Fe \quad (2)$$

The concept of using organic redox mediators to lithiate materials is not new[15], but common chemical lithiation agents such as naphthalenide lithium and biphenyl lithium typically have redox potentials close to that of $Li|Li^+$ (0.4 V and 0.3 V vs $Li|Li^+$, respectively).[16] Under such strongly reducing conditions, FeS_2 would convert beyond the desired Li_2FeS_2 form, decomposing to Fe metal and Li_2S.[17] Thus, the redox potential of any proposed lithiating agent must be sufficiently reducing to promote lithiation, but not so powerful that it forms undesirable products.[18,19] For such purposes, we select benzophenone (Ph_2CO) because of the redox potential of its single radical form, ~1.6 V vs Li/Li^+.[14] Benzophenone is otherwise well known for its reaction with sodium metal in the "ketyl still" to dry solvents such as tetrahydrofuran without the need to pull a heavy vacuum.[18] Mechanistically, Ph_2CO readily

[a] Surface Chemistry Branch, Code 6170, U.S. Naval Research Laboratory, Washington, DC 20375, USA.
[b] NRC Postdoctoral Associate at the U.S. Naval Research Laboratory, Washington, DC 20375, USA.
[c] American Society of Engineering Education Postdoctoral Associate at the U.S. Naval Research Laboratory, Washington, DC, 20375, USA
Supplementary Information available: [details of any supplementary information available should be included here]. See DOI: 10.1039/x0xx00000x

Please do not adjust margins

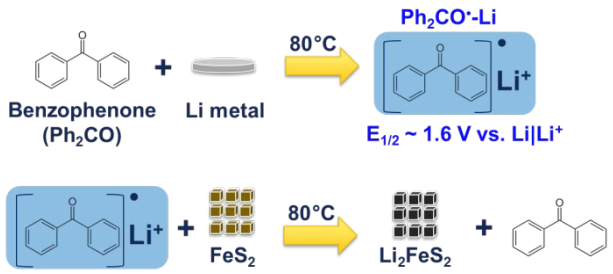

Fig. 1 Synthesis schematic of the chemical lithiation of pyrite and its transformation into Li_2FeS_2.

forms radical anions that associate with lithium or sodium metal to make a stable adduct in solution. These lithium-Ph_2CO complex exhibit a vibrant blue colour in solution and act as a visual indicator for solvent dryness.[19]

In the present synthetic process (Fig. 1) performed inside of an Ar-filled glovebox, benzophenone is dissolved into diethylene glycol dimethyl ether (diglyme), a solvent that provides a desired balance of boiling point and chemical compatibility. After complete dissolution of the benzophenone, lithium metal is added into solution such that the molar ratio of Ph_2CO:Li is 1:1. We avoid excess lithium in solution because the purple, double radical Ph_2CO:Li 1:2 adduct has a lithiating potential of ~0.8 V vs Li|Li$^+$ and will over-reduce the FeS_2.[15] This mixture is homogenized at 80°C for 4 h resulting in a deep blue solution free of any solids (Fig. S1). Next, we add commercial pyrite iron sulphide into the solution and maintain the solution temperature at 80°C for 8 h. As the lithium is removed from the Ph_2CO:Li adduct, the solution loses its blue colour and converts the grey pyrite into a black solid of chemically lithiated,

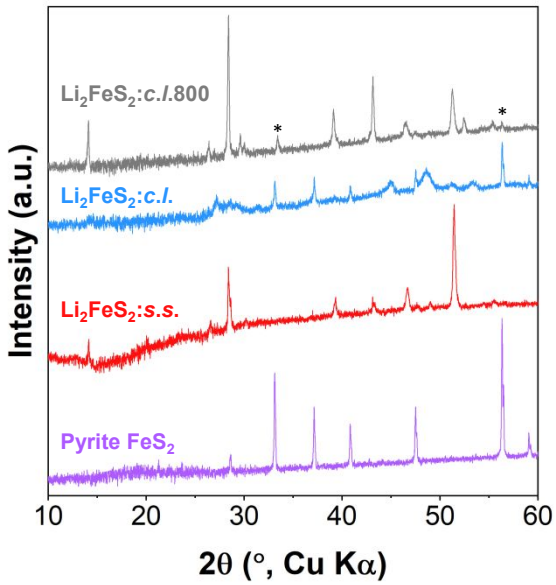

Fig. 2 X-ray diffractograms (Cu Kα radiation; λ = 1.5406 Å) of pyrite FeS_2 precursor, Li_2FeS_2:*s.s.*, Li_2FeS_2:*c.l.*, and Li_2FeS_2:*c.l.*800.

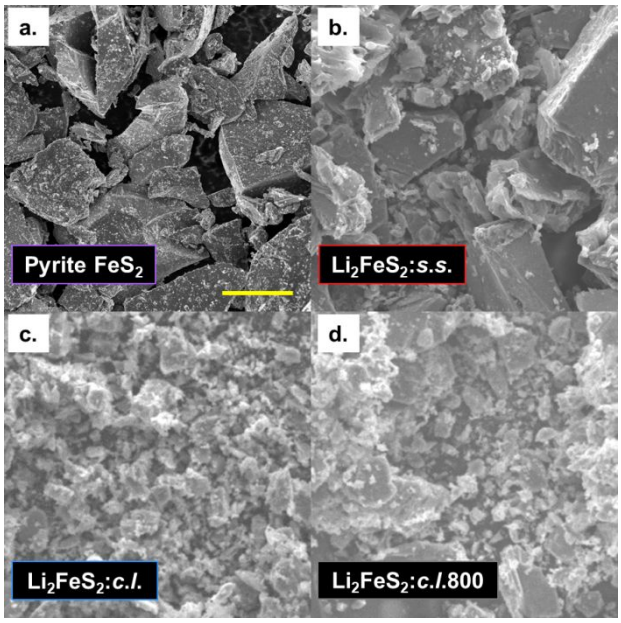

Fig. 3 Scanning electron micrographs of **a.** pyrite FeS_2 precursor, **b.** Li_2FeS_2:*s.s.*, **c.** Li_2FeS_2:*c.l.*, and **d.** Li_2FeS_2:*c.l.*800 powders. Scale bar = 25 µm

disordered Li_2FeS_2 (Li_2FeS_2:*c.l.*), evidenced by X-ray diffraction (Fig. 2) and inductively coupled plasma optical emission spectrometry (Fig. S2). A small amount of residual FeS_2 remains in the final product evidenced by the diffraction peaks near 33° and 57°. We improve the crystallinity of Li_2FeS_2:*c.l.* by heating in a graphite crucible for 16 h at 800°C, below the melting point of Li_2FeS_2 (~885 °C).[20] This process is performed entirely within the glovebox due to the severe air and moisture sensitivity of Li_2FeS_2. A graphite crucible is chosen to prevent diffusion of lithium into oxide-based crucibles. The resulting powder (Li_2FeS_2:*c.l.*800) exhibits the same P-3m1 crystallographic structure as Li_2FeS_2 synthesized via the solid-state route (Li_2FeS_2:*s.s.*),[9] albeit with different crystallographic texturing.

In contrast with the solid-state synthesis pathway, chemical lithiation of FeS_2 produces significantly smaller Li_2FeS_2 particles (tens of microns vs hundreds of nanometres), despite the >50 µm size of the commercial FeS_2 precursor (Fig. 3). The chemical lithiation of pyrite imposes significant volume change (cell volume of pyrite FeS_2: ~160 Å^3; cell volume of Li_2FeS_2: ~80 Å^3),[12,21] inducing cracking and pulverization resulting in nanoscopic Li_2FeS_2. Although the 16 h heat treatment at 800°C leads to some coarsening, Li_2FeS_2:*c.l.*800 still presents markedly smaller particles than those seen in Li_2FeS_2:*s.s.* Electrochemically active materials benefit significantly from smaller particle sizes by decreasing Li$^+$ diffusion distance and improving contact of active material to carbon powder within the composite electrode structure.[22,23] The See group demonstrates improved energy-storage capacity and cycling performance of melt-prepared $LiNaFeS_2$ through particle size reduction via cryomilling.[26]

We demonstrate the electrochemical viability of Li_2FeS_2:*c.l.*800 in a half-cell configuration using both cyclic voltammetry and

 This journal is © The Royal Society of Chemistry 20xx

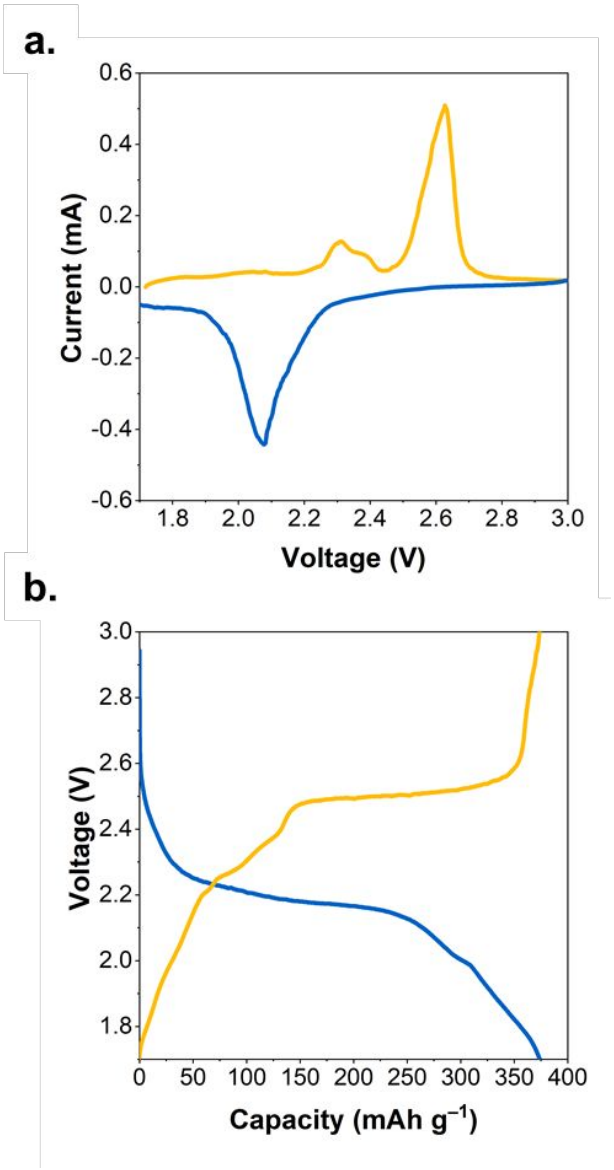

Fig. 4 a. Voltammetric sweep (0.1 mV s^{-1}) and **b.** galvanostatic charge/discharge (20 mA g^{-1}) of Li_2FeS_2:*c.l.*800 between 1.8–3.0 V in a half-cell configuration.

galvanostatic charge/discharge (Fig. 4, S3, and S4). During oxidation, we observe two distinct redox processes in the voltammogram that we ascribe to Fe^{2+}/Fe^{3+} at ~2.3 V and S^{2-}/S_2^{2} at ~2.6 V. Only one peak appears during the negative sweep suggesting concomitant iron and sulphur redox.[9] Under slow galvanostatic conditions (C/10 based on 1 e^- redox; 200 mAh g^{-1}), Li_2FeS_2:*c.l.*800 reversibly stores ~375 mAh g^{-1} or >1.8 e^-, comparable to state-of-the art performance of the material synthesized via solid-state reaction (Fig. S5).[9]

Redox-potential-matched chemical lithiation offers a versatile pathway to create lithium-rich materials. In contrast with the solid-state synthesis methods traditionally used to make Li_2FeS_2, this chemical lithiation approach produces smaller primary particles and provides an adaptable platform for compositional tuning. Adjusting the size and end groups of the polyaromatic hydrocarbon modulates the chemical potential of lithiation, affording synthetic flexibility and direct nanoscaling of various lithium-rich transition-metal sulphides.[27]

Conflicts of interest

There are no conflicts to declare.

Data availability

The data supporting this article have been included as part of the Supplementary Information.

Notes and references

1 M. Li, J. Lu, Z. Chen and K. Amine, *Advanced Materials*, 2018, **30**, 1800561.
2 A. Manthiram, J. C. Knight, S. T. Myung, S. M. Oh and Y. K. Sun, *Advanced Energy Materials*, 2015, **6**, 1501010.
3 B. Li and D. Xia, *Advanced Materials*, 2017, **29**, 1701054.
4 G. Assat and J.-M. Tarascon, *Nature Energy*, 2018, **3**, 373-386.
5 Y. Y. Hwang, J. H. Han, S. H. Park, J. E. Jung, N. K. Lee and Y. J. Lee, *Nanotechnology*, 2022, **33**, 182003.
6 J. J. Zak, S. S. Kim, F. A. L. Laskowski and K. A. See, *Journal of the American Chemical Society*, 2022, **144**, 10119-10132.
7 J. He, A. Bhargav, J. Okasinski and A. Manthiram, *Advanced Materials*, 2024, **36**, 2403521.
8 S. Saha, G. Assat, M. T. Sougrati, D. Foix, H. Li, J. Vergnet, S. Turi, Y. Ha, W. Yang, J. Cabana, G. Rousse, A. M. Abakumov and J.-M. Tarascon, *Nature Energy*, 2019, **4**, 977-987.
9 C. J. Hansen, J. J. Zak, A. J. Martinolich, J. S. Ko, N. H. Bashian, F. Kaboudvand, A. Van der Ven, B. C. Melot, J. Nelson Weker and K. A. See, *Journal of the American Chemical Society*, 2020, **142**, 6737-6749.
10 J. Barker and E. Kendrick, *Journal of Power Sources*, 2011, **196**, 6960-6963.
11 S. G. Booth, A. J. Nedoma, N. N. Anthonisamy, P. J. Baker, R. Boston, H. Bronstein, S. J. Clarke, E. J. Cussen, V. Daramalla, M. De Volder, S. E. Dutton, V. Falkowski, N. A. Fleck, H. S. Geddes, N. Gollapally, A. L. Goodwin, J. M. Griffin, A. R. Haworth, M. A. Hayward, S. Hull, B. J. Inkson, B. J. Johnston, Z. Lu, J. L. MacManus-Driscoll, X. Martínez De Irujo Labalde, I. McClelland, K. McCombie, B. Murdock, D. Nayak, S. Park, G. E. Pérez, C. J. Pickard, L. F. J. Piper, H. Y. Playford, S. Price, D. O. Scanlon, J. C. Stallard, N. Tapia-Ruiz, A. R. West, L. Wheatcroft, M. Wilson, L. Zhang, X. Zhi, B. Zhu and S. A. Cussen, *APL Materials*, 2021, **9**, 109201.
12 R. J. Batchelor, F. W. Einstein, C. H. Jones, R. Fong and J. R. Dahn, *Physical Review B: Condensed Matter and Materials Physics*, 1988, **37**, 3699-3702.
13 A. Dugast, R. Brec, G. Ouvrard and J. Rouxel, *Solid State Ionics*, 1981, **5**, 375-378.
14 R. Fong, J. R. Dahn and C. H. W. Jones, *Journal of The Electrochemical Society*, 1989, **136**, 3206-3210.
15 J. Zou, J. Zhao, B. Wang, S. Chen, P. Chen, Q. Ran, L. Li, X. Wang, J. Yao, H. Li, J. Huang, X. Niu and L. Wang, *ACS Applied Materials & Interfaces*, 2020, **12**, 44850-44857.
16 D. W. Murphy and P. A. Christian, *Science*, 1979, **205**, 651-656.
17 Y.-S. Su and J.-K. Chang, *Batteries*, 2022, **8**, 99.
18 R. Inoue, M. Yamaguchi, Y. Murakami, K. Okano and A. Mori, *ACS Omega*, 2018, **3**, 12703-12706.
19 X. Zhu, Z. Su, C. Wu, H. Cong, X. Ai, H. Yang and J. Qian, *Nano Letters*, 2022, **22**, 2956-2963.

20 C. Wu, J. Hu, H. Chen, C. Zhang, M. Xu, L. Zhuang, X. Ai and J. Qian, *Energy Storage Materials*, 2023, **60**, 102803.
21 H. Zhang, H. Wu, L. Wang, H. Xu and X. He, *Journal of Power Sources*, 2021, **492**, 229661.
22 R. A. Sharma, *Journal of The Electrochemical Society*, 1976, **123**, 448-453.
23 B. Wang, I. Braems, S. Sasaki, F. Guegan, L. Cario, S. Jobic and G. Frapper, *Journal of Physical Chemistry Letters*, 2020, **11**, 8861-8866.
24 L. Yu, X. Zhou, L. Lu, X. Wu and F. Wang, *ChemSusChem*, 2020, **13**, 5361-5407.
25 Y. Sun, N. Liu and Y. Cui, *Nature Energy*, 2016, **1**, 16071.
26 S. S. Kim, D. N. Agyeman-Budu, J. J. Zak, A. Dawson, Q. Yan, M. Cában-Acevedo, K. M. Wiaderek, A. A. Yakovenko, Y. Yao, A. Irshad, S. R. Narayan, J. Luo, J. Nelson Weker, S. H. Tolbert and K. A. See, *Chemistry of Materials*, 2022, **34**, 3236-3245.
27 R. S. Ruoff, K. M. Kadish, P. Boulas and E. C. M. Chen, *The Journal of Physical Chemistry*, 2002, **99**, 8843-8850.

 This journal is © The Royal Society of Chemistry 20xx

Data availability

The data supporting this article have been included as part of the Supplementary Information.